EARTHQUAKE ENGINEERING AND STRUCTURAL DYNAMICS
Earthquake Engng Struct. Dyn. 2001; **30**:1083–1099 (DOI: 10.1002/eqe.56)

Seismic isolation of rigid cylindrical tanks using friction pendulum bearings

Yen-Po Wang*, Min-Cheng Teng and Kuo-Whie Chung

Department of Civil Engineering, National Chiao-Tung University, 1001 Ta-Hsueh Road, Hsinchu, Taiwan

SUMMARY

Storage tanks are vulnerable to earthquakes, as numerous major earthquakes have demonstrated. The trend of recent revisions to make seismic design criteria for large-scale industrial storage tanks increasingly stringent has made development of cost-effective earthquake-resistant design and retrofit techniques for industrial tanks imperative. This study assesses the feasibility of seismic base isolation for making liquid-filled storage tanks earthquake resistant. The sliding-type friction pendulum seismic (FPS) bearings are considered rather than the elastomeric bearings because the dynamic characteristics of an FPS-isolated tank remain unchanged regardless of the storage level. This work has devised a hybrid structural-hydrodynamic model and solution algorithm, which would permit simple, accurate and efficient assessment of the seismic response of rigid cylindrical storage tanks in the context of seismic isolation. Extensive numerical simulations confirm the effectiveness of seismic base isolation of rigid cylindrical tanks using FPS bearings. Copyright © 2001 John Wiley & Sons, Ltd.

KEY WORDS: storage tanks; rigid cylindrical tanks; friction pendulum bearings

INTRODUCTION

Earthquakes may induce substantial hydrodynamic pressures on the shell wall of storage tanks, and the overturning moment caused by the lateral pressures could result in excessive compressive stresses at the bottom of one side of the tank, and hence, dynamic buckling of the shell wall [1–3]. Damage to storage tanks not only instantly disrupts essential infrastructure but can also cause fires or environmental contamination when flammable materials or hazardous chemicals leak. Given the severe damage to industrial storage tanks and the economic losses during the recent Ji–Ji earthquake ($M = 7.6$) in Taiwan, earthquake protection for such facilities has attracted serious attention in the industrial and engineering communities. Consequently, seismic design provisions for industrial tanks have become increasingly stringent and developing

* Correspondence to: Yen-Po Wang, Department of Civil Engineering, National Chiao-Tung University, 1001 Ta-Hsueh Road, Hsinchu, Taiwan.

Contract/grant sponsor: National Science Council of the Republic of China; contract/grant number: NSC 89-2211-E-009-011

Received 13 April 2000
Accepted 24 November 2000

cost-effective earthquake-resistant design and retrofit techniques for large-scale storage tanks has become crucial.

Although seismic isolation has been recognized as a promising alternative to protecting structures against earthquakes, engineering research and practices on seismic isolation of storage tanks remains limited. Unlike most structures (such as buildings or bridges), the weight of storage tanks varies in time because of variable liquid storage level, and they may contain low-temperature (e.g. LNG) or corrosive substances. Thus, rubber-type bearings, such as the lead-rubber bearings or the high-damping-rubber bearings, are not recommended for seismic isolation of storage tanks. However, friction pendulum bearings possess properties that considerably benefit the seismic isolation of industrial tanks. For instance, the fundamental period of tanks isolated by FPS bearings merely depends on the radius of curvature of the sliding interface, making dynamic characteristics of the isolated tanks invariant and fully controllable, regardless of the storage level. Being made of stainless steel, FPS bearings are also resistant to chemicals, fires, temperature extremes, and adverse environmental exposure. Given the above advantages, FPS seismic bearings are better for industrial tank applications. So far, application of seismic isolation to industrial tanks has mostly used friction pendulum bearings [4].

Whereas the response to earthquakes of base fixed (or anchored) liquid-filled tanks on rigid or flexible foundations has been the subject of numerous studies in previous literature [5–10], little information exists on the corresponding response of tanks with seismic isolation using sliding-type bearings. The presence of frictions, with highly non-linear characteristics, of the sliding bearings has made the problems more complex. This study devises a hybrid structural-hydrodynamic model and solution algorithm, which would permit simple, accurate and efficient assessment of the seismic response of rigid cylindrical storage tanks in the context of seismic isolation. The effectiveness of seismic base isolation of rigid cylindrical tanks using friction pendulum bearings is verified through extensive numerical simulations under the 1940 El Centro Earthquake. Furthermore, the effects of the geometric properties (height-to-radius ratio) of the tank, and earthquake intensity, on seismic response control efficiency are investigated. Through regressive analyses, empirical formula are developed to estimate the control efficiency of seismic isolation, in terms of peak reduction of the base shear or the overturning moment, with respect to the geometrical properties of the tanks, earthquake intensity, and the frictional coefficient of the bearings. Finally, design charts for predicting the maximum sliding displacement of the FPS bearings of the corresponding design parameters are also presented.

ANALYTICAL MODELLING

Review of the hydrodynamics within rigid tanks

A rigid, circular cylindrical tank defined by a cylindrical coordinate system, with r, θ, and z denoting, respectively, the radial, circumferential, and axial co-ordinates, is filled with liquid to a storage level H, as illustrated in Figure 1. The liquid with density ρ, is assumed to be incompressible, irrotational and inviscid. Under horizontal earthquake ground acceleration, $\ddot{x}_g(t)$, in the direction $\theta = 0$, the velocity potential function, $\varphi(r, \theta, z, t)$, of the liquid flow within the tank

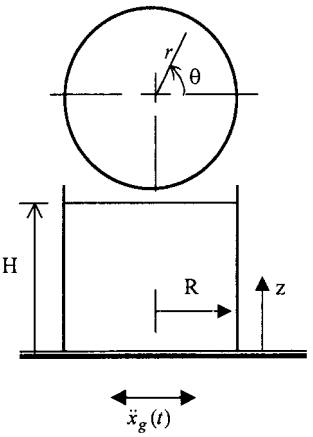

Figure 1. Configuration of the cylindrical tank.

satisfies the Laplace's equation [7] as

$$\frac{\partial^2\varphi}{\partial r^2}+\frac{1}{r}\frac{\partial\varphi}{\partial r}+\frac{1}{r^2}\frac{\partial^2\varphi}{\partial\theta^2}+\frac{\partial^2\varphi}{\partial z^2}=0 \tag{1}$$

The flow velocity in the direction of a generalized n co-ordinate, $v_n(r,\theta,z,t)$, is given by $v_n=\partial\varphi/\partial n$ and the hydrodynamic pressure, $p(r,\theta,z,t)$, is given by $p=\rho\partial\varphi/\partial t$.

The solution of the Laplace's equation (1) must satisfy the following boundary conditions:

$$-\left.\frac{\partial\varphi}{\partial z}\right|_{z=0}=0 \tag{2a}$$

because the vertical component of the liquid velocity must be zero at the tank base ($z=0$);

$$-\left.\frac{\partial\varphi}{\partial r}\right|_{r=R}=\dot{x}_{\mathrm{g}}\cos\theta \tag{2b}$$

since the radial velocities of the liquid and the rigid tank wall must be consistent along the tank wall ($r=R$), where $\dot{x}_{\mathrm{g}}$ is the velocity of the horizontal ground motion;

$$\rho g d(r,\theta,t)=\rho\left.\frac{\partial\varphi}{\partial t}\right|_{z=H} \tag{2c}$$

if the vertical inertia of the surface waves is neglected, where $d(r,\theta,t)$ is the sloshing displacement measured from the quiescent liquid-free surface ($z=H$), and g is the gravitational acceleration;

$$-\left.\frac{\partial\varphi}{\partial z}\right|_{z=H}=\frac{\partial d}{\partial t} \tag{2d}$$

for compatibility of the vertical velocity at the free surface.

The solution of Equation (1) can be conveniently expressed by superpositioning two components as

$$\varphi(r,\theta,z,t)=\varphi_1(r,\theta,z,t)+\varphi_2(r,\theta,z,t) \tag{3}$$

where φ_1 is associated with the portion of the liquid that varies in synchronization with the rigid tank, and φ_2 is associated with the hydrodynamic motion of the liquid relative to the tank.

Accordingly, $\partial\varphi_1/\partial z=0$ since the tank is subjected to horizontal ground excitation only. Boundary condition (2a) can further be revised as $\partial\varphi_2/\partial z|_{z=0}=0$, condition (2b) as $\partial\varphi_1/\partial r|_{r=R}=-\dot{x}_g(t)\cos\theta$ and $\partial\varphi_2/\partial r|_{r=R}=0$, and condition (2d) as $-\partial\varphi_2/\partial z|_{z=H}=\partial d/\partial t$. Solution φ_1 can immediately be obtained as

$$\varphi_1=-\dot{x}_g(t)r\cos\theta \tag{4}$$

and φ_2 from Equations (1) and (4) by the method of separation of variables along with the boundary condition, $\partial\varphi_2/\partial r|_{r=R}=0$, giving

$$\varphi_2(\xi,\theta,\eta,t)=\sum_{j=1}^{\infty}\left[A(t)\cosh\lambda_j\eta+B(t)\sinh\lambda_j\eta\right]J_1(\lambda_j\xi)\cos\theta \tag{5}$$

where $\xi=r/R$, $\eta=z/R$, J_1 is the Bessel function of the first kind and λ_j is the jth root of $J_1'(\lambda)=0$. $A(t)$ and $B(t)$ are time-dependent coefficients to be determined from the remaining boundary conditions. Meanwhile, the sloshing displacement $d(\xi,\theta,t)$ on the free surface may be shown proportional to $J_1(\lambda_j\xi)\cos\theta$ as

$$d(\xi,\theta,t)=\sum_{j=1}^{\infty}D_j(t)\frac{J_1(\lambda_j\xi)}{J_1(\lambda_j)}\cos\theta,\quad j=1,\ldots,\infty \tag{6}$$

where $D_j(t)$ represents the position of the free surface of the liquid at the junction with the tank wall ($\xi=1,\theta=0$) when the surface wave is sloshing in its jth mode. With boundary conditions $\partial\varphi_2/\partial\eta|_{\eta=0}=0$ and $-\partial\varphi_2/\partial\eta|_{\eta=\alpha}=\partial d/\partial t$, where $\alpha=H/R$, φ_2 can be written in the form

$$\varphi_2(\xi,\theta,\eta,t)=-\sum_{j=1}^{\infty}\frac{R}{\lambda_j}\left[\frac{\dot{D}_j(t)\cosh\lambda_j\eta}{\sinh\lambda_j\alpha}\right]\frac{J_1(\lambda_j\xi)}{J_1(\lambda_j)}\cos\theta,\quad j=1,\ldots,\infty \tag{7}$$

Using boundary condition (2c) and the orthogonality of the Bessel functions, the hydrodynamic equation is then established as

$$\ddot{D}_j(t)+\omega_j^2D_j(t)=-\varepsilon_j\lambda_j\tanh(\lambda_j\alpha)\ddot{x}_g,\quad j=1,\ldots,\infty \tag{8}$$

where $\omega_j^2=(\lambda_j g/R)\tanh\lambda_j\alpha$ and $\varepsilon_j=2/(\lambda_j^2-1)$.

Meanwhile, the hydrodynamic pressure, $p(\xi,\theta,\eta,t)$, on the tank wall can be obtained as

$$p(1,\theta,\eta,t)=\rho\left.\frac{\partial\varphi}{\partial t}\right|_{\xi=1}=-\rho R\cos\theta\left\{\ddot{x}_g(t)+\sum_{j=1}^{\infty}\left[\frac{\ddot{D}_j(t)\cosh\lambda_j\eta}{\lambda_j\sinh\lambda_j\alpha}\right]\right\} \tag{9}$$

which can be further divided into the impulsive, p^i, and the convective, p^c, components using Equation (8) as

$$p=p^i+p^c \tag{10}$$

where

$$p^{\mathrm{i}} = -\rho R\cos\theta\left[1-\sum_{j=1}^{\infty} C_j^2\frac{\varepsilon_j\cosh(\lambda_j\eta)}{\sinh(\lambda_j\alpha)}\right]\ddot{x}_{\mathrm{g}}(t) \tag{11a}$$

and

$$p^{\mathrm{c}} = \rho R\cos\theta\left[\sum_{j=1}^{\infty} C_j^2\frac{\varepsilon_j\cosh(\lambda_j\eta)}{\sinh(\lambda_j\alpha)}\right]\frac{\omega_j^2 D_j(t)}{\varepsilon_j\lambda_j\tanh(\lambda_j\alpha)} \tag{11b}$$

in which $C_j^2 = (R/g\lambda_j)\omega_j^2$. Once the pressure is derived, the instantaneous base shear, $S(t)$, of the tank can be calculated as

$$S(t) = \int_0^{\alpha}\int_0^{2\pi} p(1,\theta,\eta,t)R^2\cos\theta\,\mathrm{d}\theta\,\mathrm{d}\eta = -m_0\ddot{x}_{\mathrm{g}}(t) + \sum_{j=1}^{\infty} m_j\frac{\omega_j^2 D_j(t)}{\varepsilon_j\lambda_j\tanh(\lambda_j\alpha)} \tag{12}$$

in which $m_0 = m_l(1-\sum_{j=1}^{\infty} C_j^2\varepsilon_j/\lambda_j\alpha)$, with $m_l = \rho R^2\pi H$, is the equivalent impulsive mass of the liquid that is moving synchronously with the rigid tank, and $m_j = m_l C_j^2\varepsilon_j/\lambda_j^2\alpha$ is the modal mass of the liquid corresponding to the jth mode of the convective motion. Similarly, the overturning moment, $M_{\mathrm{OT}}(t)$, can be calculated as

$$M_{\mathrm{OT}}(t) = \int_0^{\alpha}\int_0^{2\pi} p(1,\theta,\eta,t)\eta R^3\cos\theta\,\mathrm{d}\theta\,\mathrm{d}\eta = -m_0 h_0\ddot{x}_{\mathrm{g}}(t) + \sum_{j=1}^{\infty} m_j h_j\frac{\omega_j^2 D_j(t)}{\varepsilon_j\lambda_j\tanh(\lambda_j\alpha)} \tag{13}$$

where

$$h_0 = H\left\{\frac{1}{2}-\sum_{j=1}^{\infty}\left(\frac{C_j^2\varepsilon_j(1-\cosh\lambda_j\alpha)}{\lambda_j^2\alpha^2\sinh\lambda_j\alpha}+\frac{C_j^2\varepsilon_j}{\lambda_j\alpha}\right)\right\}\Bigg/\left(1-\sum_{j=1}^{\infty}\frac{C_j^2\varepsilon_j}{\lambda_j\alpha}\right)$$

and

$$h_j = H\left\{\left(\frac{C_j^2\varepsilon_j(1-\cosh\lambda_j\alpha)}{\lambda_j^2\alpha^2\sinh\lambda_j\alpha}+\frac{C_j^2\varepsilon_j}{\lambda_j\alpha}\right)\right\}\Bigg/\left(\frac{C_j^2\varepsilon_j}{\lambda_j\alpha}\right)$$

Notably,

$$m_l = m_0 + \sum_{j=1}^{\infty} m_j \tag{14}$$

The base shear and overturning moment are central to the earthquake-resistant design of storage tanks and will be examined to verify the effectiveness of seismic isolation. The hydrodynamic system (8) can be revised for each mode as an analogy of a single-degree-of-freedom base-excited spring-mass system as

$$m_j\ddot{\bar{D}}_j(t) + k_j\bar{D}_j(t) = -m_j\ddot{x}_{\mathrm{g}}(t), \quad j = 1,\ldots,\infty \tag{15}$$

where $\bar{D}_j(t) = D_j(t)/(\varepsilon_j\lambda_j\tanh\lambda_j\alpha)$ and $k_j = \omega_j^2 m_j$. By considering only the first N modes, the hydrodynamic system due to ground excitations can be concisely expressed as

$$\mathbf{M}_{\mathrm{s}}\ddot{\bar{\mathbf{D}}}(t) + \mathbf{K}_{\mathrm{s}}\bar{\mathbf{D}}(t) = -\mathrm{M}_{\mathrm{s}}\mathbf{1}\ddot{x}_{\mathrm{g}} \tag{16}$$

where $\bar{\mathbf{D}} = [\bar{D}_1 \cdots \bar{D}_N]^{\mathrm{T}}$ is the $N \times 1$ generalized displacement vector of the convective motion (relative to the tank);

$$\mathbf{M}_{\mathrm{s}} = \begin{bmatrix} m_1 & & \\ & \ddots & \\ & & m_N \end{bmatrix}$$

is the $N \times N$ generalized mass matrix of the convective motion;

$$\mathbf{K}_{\mathrm{s}} = \begin{bmatrix} k_1 & & \\ & \ddots & \\ & & k_N \end{bmatrix}$$

is the $N \times N$ generalized stiffness matrix of the liquid, and $\mathbf{1}$ denotes the $N \times 1$ uniform vector with all its entries being 1.

Hybrid structural-hydrodynamic systems of base-isolated rigid tanks

When FPS are installed beneath its base for seismic isolation, the rigid tank and the liquid it contains will slide together during earthquakes (Figure 2(a)). The kinetic energy (T) and the potential energy (V) of the hybrid structural-hydrodynamic system are defined, respectively, as

$$T = [\dot{\bar{\mathbf{D}}} + \mathbf{1}(\dot{x}_{\mathrm{b}} + \dot{x}_{\mathrm{g}})]^{\mathrm{T}} \mathbf{M}_{\mathrm{s}} [\dot{\bar{\mathbf{D}}} + \mathbf{1}(\dot{x}_{\mathrm{b}} + \dot{x}_{\mathrm{g}})] + \tfrac{1}{2} m_{\mathrm{b}} (\dot{x}_{\mathrm{b}} + \dot{x}_{\mathrm{g}})^2 \tag{17a}$$

and

$$V = \frac{1}{2} \bar{\mathbf{D}}^{\mathrm{T}} \mathbf{K}_{\mathrm{s}} \bar{\mathbf{D}} + m_{\mathrm{t}} g R_{\mathrm{FPS}} (1 - \cos\gamma) \cong \frac{1}{2} \bar{\mathbf{D}}^{\mathrm{T}} \mathbf{K}_{\mathrm{s}} \bar{\mathbf{D}} + \frac{1}{2} \frac{m_{\mathrm{t}}}{R_{\mathrm{FPS}}} x_{\mathrm{b}}^2 \tag{17b}$$

where x_{b} and $\dot{x}_{\mathrm{b}}$ are, respectively, the sliding displacement and sliding velocity of the base (relative to the ground), m_{b} is the effective mass of the tank, including the mass of the tank itself and the equivalent impulsive mass (m_0) of the liquid; $m_{\mathrm{t}} = \sum_{j=1}^{N} m_j + m_{\mathrm{b}}$ is the total mass of the hybrid system; R_{FPS} is the radius of curvature of the sliding surface and $\gamma \cong x_{\mathrm{b}}/R_{\mathrm{FPS}}$ is the sliding angle around the center of curvature as depicted in Figure 2(b). Considering the friction force, $f(t)$, between the sliding interfaces of the bearing as a non-conservative force, the equation of motion of the hybrid system can be derived by applying the Lagrange's equation [11] as

$$\mathbf{M}\ddot{\mathbf{x}}(t) + \mathbf{K}\mathbf{x}(t) = -\mathbf{E}\ddot{x}_{\mathrm{g}}(t) + \mathbf{B}f(t) \tag{18}$$

where

$$\mathbf{x}(t) = \begin{pmatrix} \bar{\mathbf{D}}(t) \\ x_{\mathrm{b}}(t) \end{pmatrix}$$

is the $(N+1) \times 1$ displacement vector;

$$\mathbf{M} = \begin{bmatrix} \mathbf{M}_{\mathrm{s}} & \mathbf{M}_{\mathrm{s}}\mathbf{1} \\ \mathbf{1}^{\mathrm{T}}\mathbf{M}_{\mathrm{s}} & \mathbf{1}^{\mathrm{T}}\mathbf{M}_{\mathrm{s}}\mathbf{1} + m_{\mathrm{b}} \end{bmatrix}$$

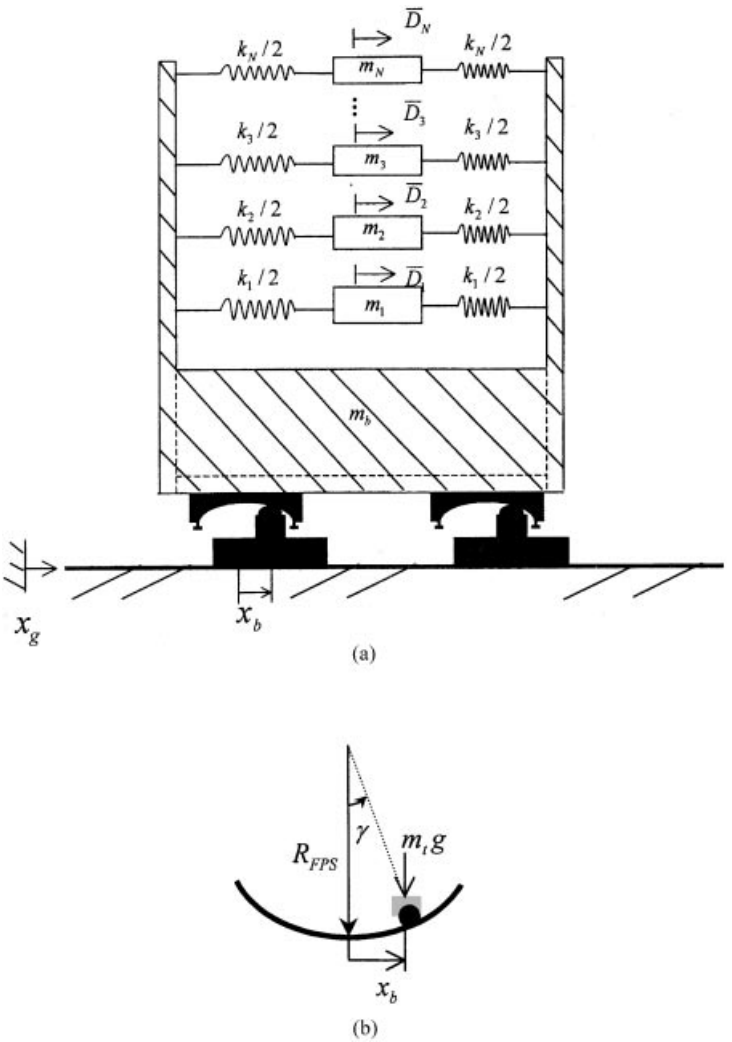

Figure 2. (a) Tank isolated with friction pendulum seismic bearings and (b) pendulum mechanism.

is the $(N+1)\times(N+1)$ mass matrix,

$$\mathbf{K}=\begin{bmatrix}\mathbf{K}_s & \mathbf{0}\\ \mathbf{0} & \frac{m_t g}{R}\end{bmatrix}$$

is the $(N+1)\times(N+1)$ stiffness matrix,

$$\mathbf{E}=\begin{pmatrix}\mathbf{M}_s\mathbf{1}\\ \mathbf{1}^T\mathbf{M}_s\mathbf{1}+m_b\end{pmatrix}$$

is the $(N+1)\times 1$ location matrix of the earthquake load, and

$$\mathbf{B}=\begin{pmatrix}\mathbf{0}\\1\end{pmatrix}$$

is the $(N+1)\times 1$ location matrix of the friction force.

By assuming small sliding displacement ($\gamma \ll 1$), the friction force, f, acting along the sliding surfaces is governed by

$$|f| \leqslant \mu m_t g \tag{19}$$

where μ is the friction coefficient. The non-sliding conditions for the bearings are

$$|f| < \mu m_t g \quad \text{and} \quad \dot{x}_b = 0 \tag{20}$$

and sliding occurs only if

$$f = \mu m_t g \,\mathrm{sgn}(\dot{x}_b) \quad \text{and} \quad \dot{x}_b \neq 0 \tag{21}$$

where sgn denotes the signum function. The hybrid structural-hydrodynamic system (18) is highly non-linear because of friction. A numerical procedure based on the concept of shear balance at the sliding interfaces [12, 13] is developed in the following section to solve this non-linear dynamic problem.

SOLUTION ALGORITHM FOR HYBRID STRUCTURAL-HYDRODYNAMIC SYSTEMS WITH SLIDING MOTION

Equation (18) can be represented in a state-space form, leading to a first-order differential equation as

$$\dot{\mathbf{z}}(t) = \mathbf{A}^*\mathbf{z}(t) + \mathbf{E}^*\ddot{x}_g(t) + \mathbf{B}^* f(t) \tag{22}$$

where

$$\mathbf{z}(t) = \begin{bmatrix}\mathbf{x}(t)\\ \dot{\mathbf{x}}(t)\end{bmatrix}$$

is the $2(N+1)\times 1$ state vector,

$$\mathbf{A}^* = \begin{bmatrix}\mathbf{0} & \mathbf{I}\\ -\mathbf{M}^{-1}\mathbf{K} & \mathbf{0}\end{bmatrix}$$

is the $2(N+1)\times 2(N+1)$ system matrix,

$$\mathbf{B}^* = \begin{bmatrix}\mathbf{0}\\ \mathbf{M}^{-1}\mathbf{B}\end{bmatrix}$$

is the $2(N+1)\times 1$ friction-loading matrix and

$$\mathbf{E}^* = \begin{bmatrix} \mathbf{0} \\ \mathbf{M}^{-1}\mathbf{E} \end{bmatrix}$$

is the $2(N+1)\times 1$ external loading matrix.

With first-order interpolations of the loading terms between two consecutive sampling instants, the state equation (22) can further be resolved as a difference equation to be

$$\mathbf{z}[k] = \mathbf{A}\mathbf{z}[k-1] + \mathbf{B_0} f[k-1] + \mathbf{B_1} f[k] + \mathbf{E_0}\ddot{x}_g[k-1] + \mathbf{E_1}\ddot{x}_g[k] \tag{23}$$

where
$\mathbf{A} = e^{\mathbf{A}^*\Delta t}$ is the $2(N+1)\times 2(N+1)$ discrete-time system matrix with Δt being the integration time step,
$\mathbf{B_0} = [(\mathbf{A})^{-1}\mathbf{A} + (1/\Delta t)(\mathbf{A})^{-2}(\mathbf{I}-\mathbf{A})]\mathbf{B}$ is the $2(N+1)\times 1$ discrete-time friction-loading matrix of the previous time step,
$\mathbf{B_1} = [-(\mathbf{A})^{-1} + (1/\Delta t)(\mathbf{A})^{-2}(\mathbf{A}-\mathbf{I})]\mathbf{B}$ is the $2(N+1)\times 1$ discrete-time friction-loading matrix of the current time step,
$\mathbf{E_0} = [(\mathbf{A})^{-1}\mathbf{A} + (1/\Delta t)(\mathbf{A})^{-2}(\mathbf{I}-\mathbf{A})]\mathbf{E}$ is the $2(N+1)\times 1$ discrete-time external loading matrix of the previous time step, and
$\mathbf{E_1} = [-(\mathbf{A})^{-1} + (1/\Delta t)(\mathbf{A})^{-2}(\mathbf{A}-\mathbf{I})]\mathbf{E}$ is the $2(N+1)\times 1$ discrete-time external loading matrix of the current time step.

The discrete-time state-space equation (23) indicates that, the friction force, $f[k]$, of the current time instant depends on the motion conditions, which are not known as *a priori*. Therefore, the solution cannot be obtained directly through simple recursive calculations.

During the slip phases, the friction force is known as defined by Equation (21), but the sliding velocity remains unknown. Meanwhile, during the stick phases, the sliding velocity at the base floor is zero, as defined by Equation (20), but the friction force (or equivalently, the base shear) remains undetermined. Restated, either the friction force or the sliding velocity is known, depending on the motion condition. This extra condition allows the friction force, $f[k]$, at time k to be uniquely determined.

Initially, for time instant k, granting a stick condition for the isolated tank gives

$$\dot{x}_b[k] = \mathbf{D}\mathbf{z}[k] = 0 \tag{24}$$

where $\mathbf{D} = [\mathbf{0}\ \mathbf{B}^T]$ is the $1\times 2(N+1)$ location vector of the base velocity, $\dot{x}_b[k]$. Substituting Equation (23) for $\mathbf{z}[k]$ into Equation (24), the expected base shear, $\bar{f}[k]$, which would prevent the tank from sliding can be resolved in a closed form as

$$\bar{f}[k] = -(\mathbf{D}\mathbf{B}_1)^{-1}\mathbf{D}(\mathbf{A}\mathbf{z}[k-1] + \mathbf{E}_0\mathbf{w}[k-1] + \mathbf{E}_1\mathbf{w}[k] + \mathbf{B}_0 f[k-1]) \tag{25}$$

which, according to the friction law, should be less than the maximum friction force. Now, if $|\bar{f}[k]| < \mu m_t g$, then the stick condition granted initially in the analysis is correct, and the actual friction force is updated by $f[k] = \bar{f}[k]$; otherwise, the tank should be in the slip phase instead, and the friction force is corrected in accordance with $f[k] = \mu W\,\mathrm{sgn}(\bar{f}[k])$. With the friction force determined, the response, $\mathbf{z}[k]$, of the isolated tank is obtained from Equation (23).

The friction force is determined, with the extra conditions of equilibrium and kinematic compatibility at the sliding interfaces, by simple matrix algebraic analysis under the framework

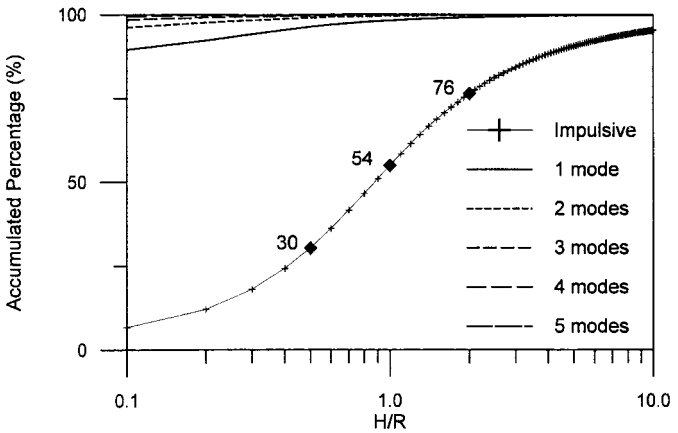

Figure 3. Accumulated modal participation factors of the hydrodynamic system.

of state-space formulation. The structural-hydrodynamic responses are thus obtained recursively with a one-step correction strategy, and a constant integration step size can be used throughout the analysis, without slowing down even near the stick–slip transitions.

NUMERICAL EXAMPLE

Consider a cylindrical rigid tank with radius (R) of 3 m, height of 7 m and weight of 65.2 kN. Containing liquid of density $\rho = 800\,\text{kg/m}^3$, the tank is to be isolated using FPS bearings with a radius of curvature $R_{\text{FPS}} = 1\,\text{m}$ so that the fundamental period of the isolated tank during sliding is shifted to 2 s, regardless of the storage level. The 1940 El Centro earthquake serves as the input to verify the effectiveness of seismic isolation using FPS bearings. The integration time step of 0.01 s, which is considered large in the context of non-linear dynamic analysis, is used throughout the numerical simulations.

For an efficient and accurate analysis, the hydrodynamic system (16) should include sufficient vibration modes. According to Figure 3, the curves of the accumulated percentage of modal participation factors with respect to the height-to-radius ratio (H/R) indicate that, over 99 per cent of the hydrodynamic motion is sufficiently covered by the first five modes, regardless of the H/R ratio. Therefore, the following analyses only account for the first five modes of the hydrodynamic motion. Figure 4 illustrates the corresponding mode shapes of the surface sloshing along the direction of $\theta = 0$. The centre of the circular cross-section is a nodal point for every mode, without exception, because of the cylindrical symmetry of the tank.

Effectiveness of seismic isolation of the storage tanks is first verified by investigating the dynamic pressure exerted on the tank wall during the earthquake. Figures 5–7 illustrate the profiles of the dynamic pressure distribution, with and without seismic isolation, on the tank wall ($r = R, \theta = 0$) for $H/R = 2, 1$ and 0.5, respectively. With seismic isolation, the impulsive pressure is significantly reduced (Figures 5(a), 6(a) and 7(a)) while the convective pressure remains virtually unchanged (Figures 5(b), 6(b) and 7(b)) so that the overall dynamic

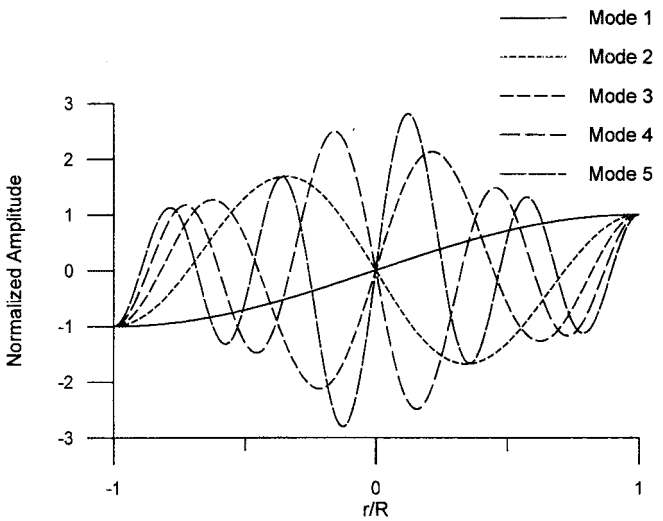

Figure 4. Mode shapes of the surface sloshing.

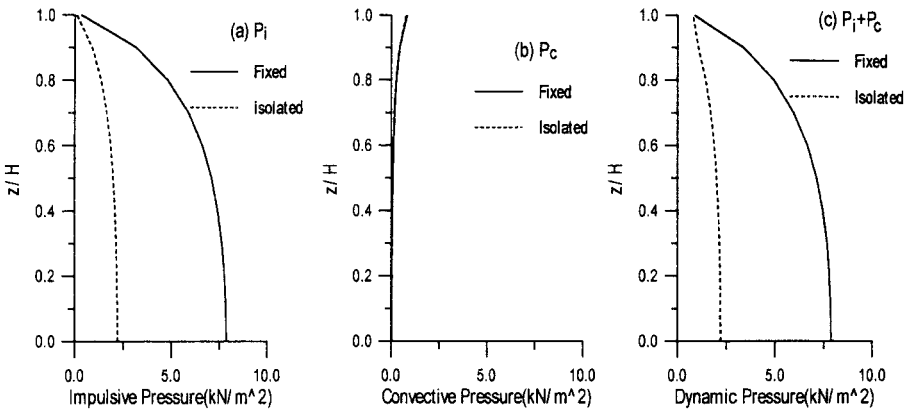

Figure 5. Distribution of dynamic pressure on the tank wall ($\theta = 0$, $H/R = 2$).

pressure is depressed (Figures 5(c), 6(c) and 7(c)). This result confirms the effectiveness of seismic isolation. Notably, the dynamic pressure comes mainly from the impulsive part, and the proportion of the impulsive pressure to the dynamic pressure increases with H/R. The latter phenomena can be explained by the modal participation factors in Figure 3, where the proportion of the impulsive mass in the hydrodynamic system increases with H/R.

The time histories of the base shear (with and without isolation), normalized with respect to the total weight of the storage tank, $W = m_t g$, are shown in Figure 8(a) for $H/R = 2$. When the tank is isolated with an FPS of 5 per cent of frictional coefficient, a significant reduction on the base shear is observed during the entire history and a peak reduction of over 70 per

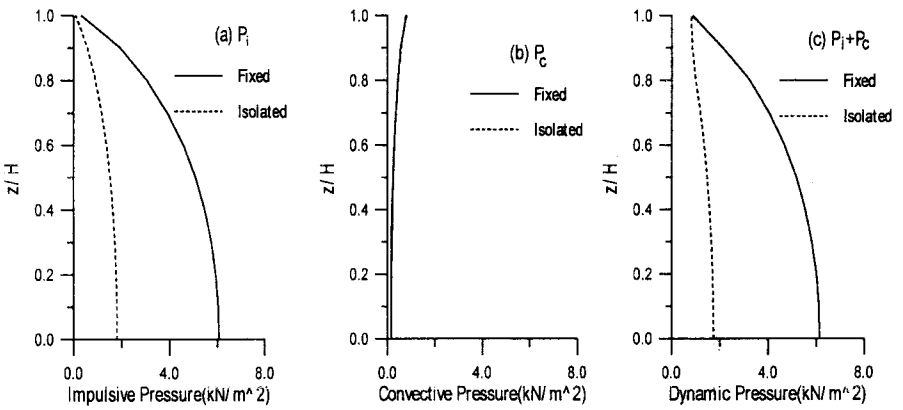

Figure 6. Distribution of dynamic pressure on the tank wall ($\theta = 0$, $H/R = 1$).

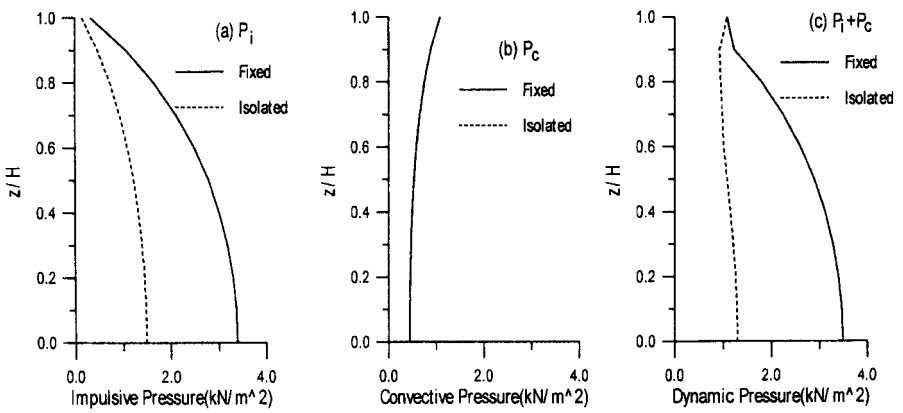

Figure 7. Distribution of dynamic pressure on the tank wall ($\theta = 0, H/R = 1/2$).

cent is achieved. The overturning moment, which is normalized with respect to the product of the total weight of the tank and the storage level (WH), exhibits the same trend, as illustrated in Figure 8(b). Results for both the representative design parameters indicate that seismic isolation significantly improves the earthquake resistance of the tank. Notably, the isolated tank cannot rock since the inequality

$$\left|\frac{M_{\mathrm{OT}}}{WH}\right| < \frac{1}{H/R} = 0.5 \tag{26}$$

holds for the entire response history. However, no evident change to the hydrodynamics has been observed, as indicated from the sloshing displacement, d, at the junction of the free surface with the tank wall along the axis of $\theta = 0$. This behaviour is natural since the fundamental period of the convective motion appears to be long (about 2.5 s in this case) and thus the sloshing response is not much affected by seismic isolation, which effectively aims to

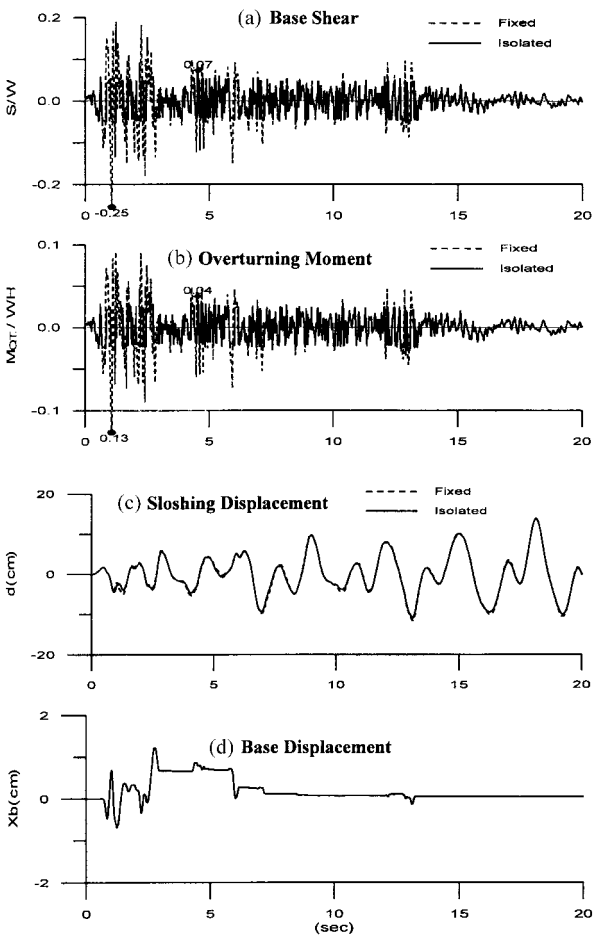

Figure 8. Seismic response analysis of tank–liquid system w/ and w/o base isolation ($H/R = 2$, $\mu = 5$ per cent).

filter out the responses of relatively higher frequencies. Figure 8(d) illustrates the time history of the sliding displacement of the FPS bearing, and the maximum reads only 1.2 cm even under a strong earthquake. The isolation system can be easily designed to accommodate this displacement.

To further understand the dynamic characteristics of the tank–liquid system with seismic isolation, a series of parametric studies is conducted by considering the effects of earthquake intensity (in terms of the peak ground acceleration, PGA), frictional coefficient (μ), and height-to-radius ratio (H/R). A storage tank with $H/R = 2$ is examined first.

Figure 9(a) shows the peak reduction factor of the overturning moment (β_M) with respect to the dimensionless factor PGA/μg for various frictional coefficients of the sliding bearing, and the figure finds that, variations between the curves for different frictional coefficients

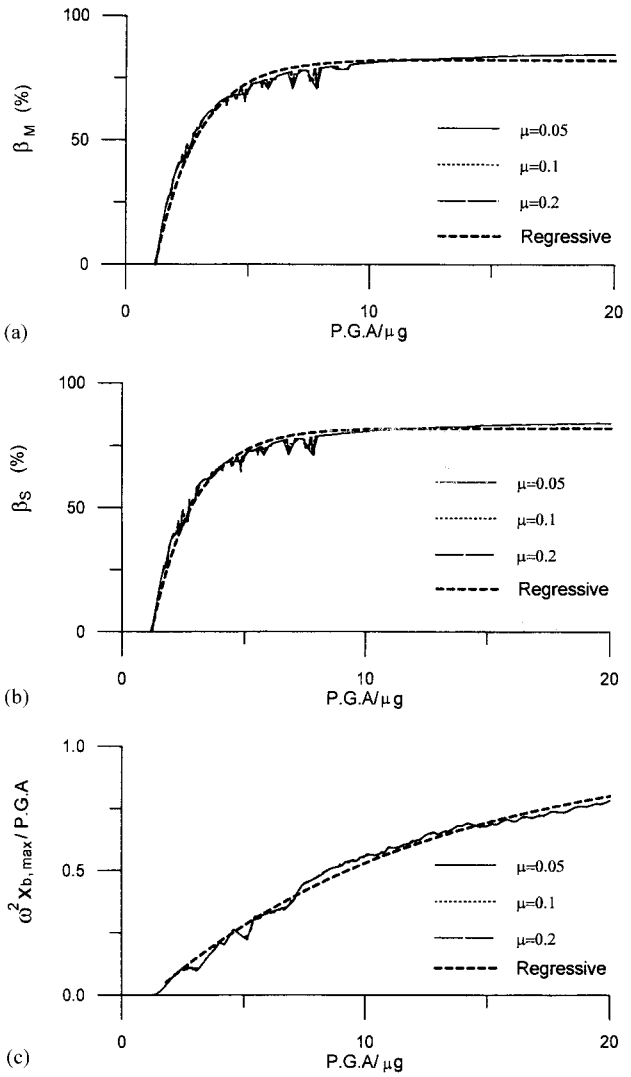

Figure 9. (a) Peak reduction of overturning moment ($H/R=2$). (b) Peak reduction of base shear ($H/R=2$). (c) Normalized maximum base displacement ($H/R=2$).

are negligible. The reduction factor increases with PGA/μg and approaches about 80 per cent asymptotically. This pattern implies that, for a given friction level, the stronger the earthquake, the more effective the isolation system. This behaviour can also be interpreted as meaning that, for a given earthquake intensity, the smaller the frictional coefficient, the better the isolation performance. Regressive analysis establishes an empirical formula for β_M as

$$\beta_M = 82.4[1 - e^{-0.57(PGA/\mu g - 1.2)}] \tag{27}$$

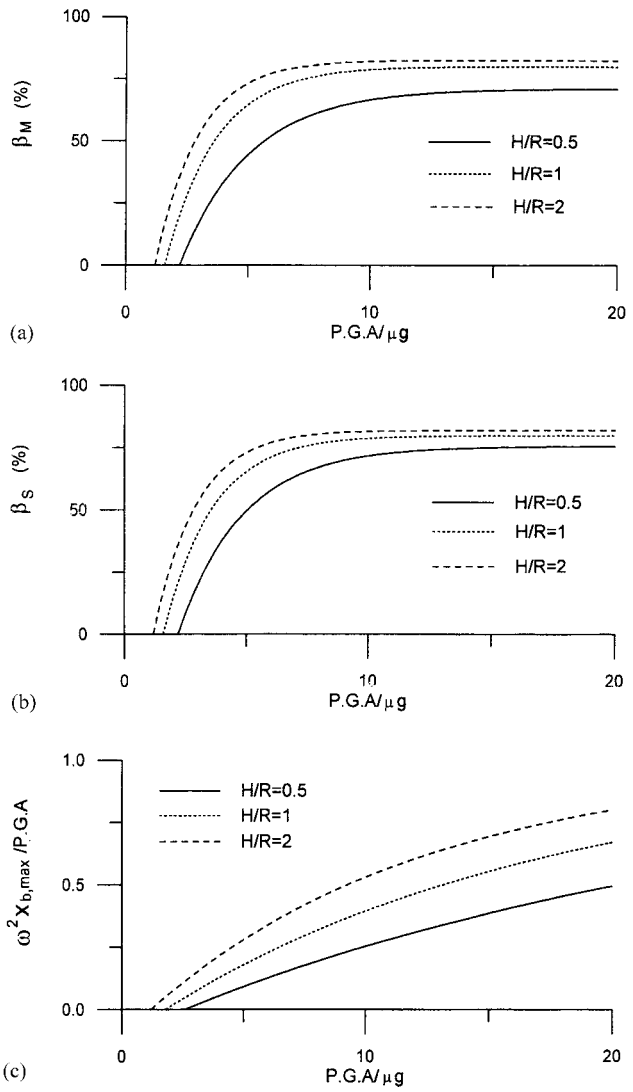

Figure 10. (a) Peak reduction of overturning moment. (b) Peak reduction of base shear. (c) Normalized maximum base displacement.

from which the control efficiency of seismic isolation on the tank can be estimated for a specified earthquake intensity and a frictional coefficient of the FPS.

Figure 9(b) shows the peak reduction factor of the base shear (β_S) with respect to the dimensionless factor PGA/μg for various frictional coefficients of the sliding bearing. The reduction factor increases with PGA/μg and approaches 80 per cent asymptotically, as with the behavior which resembles that of the overturning moment. Again, variations between the

results for different frictional coefficients are negligible. Similarly, an empirical formula is established for β_S as

$$\beta_S = 81.9[1 - e^{-0.58(PGA/\mu g - 1.2)}] \tag{28}$$

Figure 9(c) shows the normalized maximum base displacement, $\omega^2 x_{b,max}/PGA$, with respect to the dimensionless factor, $PGA/\mu g$ for various frictional coefficients of the sliding bearing, where $\omega = \sqrt{g/R_{FPS}}$ is the fundamental frequency of the isolated tank and $x_{b,max}$ is the maximum base displacement. Again the curves for different frictional coefficients are found to be largely the same. The normalized maximum base displacement is found to increase with $PGA/\mu g$. This behaviour means that for a given friction level, the stronger the earthquake, the further the bearings slide. Or conversely, for a given earthquake intensity, the sliding displacement decreases with increasing frictional coefficient. This behaviour is reasonable since the friction mechanism dissipates energy and thus helps limit the sliding displacement. An empirical formula is established for the normalized maximum displacement by regressive analysis as

$$\frac{\omega^2 x_{b,max}}{PGA} = 1 - e^{-0.086(PGA/\mu g - 1.2)} \tag{29}$$

from which the maximum base displacement for various dynamic systems can be estimated for a specified earthquake intensity and a frictional coefficient. The displacement bound, $x_{b,max}$, serves as the basis for sizing the isolation system in the preliminary design stage.

The effect of the height-to-radius ratio on seismic isolation of the tanks is further investigated as what follows. Figures 10(a) and (b) illustrate the regression curves of the peak reduction of the overturning moment and the base shear, respectively, with respect to $PGA/\mu g$ for various height-to-radius ratios ($H/R = 0.5, 1$ and 2). Evidently, higher storage level implies a more effective isolation performance. This result is consistent with the previous observation from Figure 3 that, the proportion of the impulsive mass in the entire hydrodynamic system increases with H/R and seismic isolation is most effective for this portion. On the other hand, the normalized base displacement with respect to the dimensionless factor $PGA/\mu g$ in Figure 10(c) reveals that, for a specified $PGA/\mu g$, higher storage level implies greater sliding distance. Results for other H/R ratios, if desired, may then be approximated from the three curves by interpolation or extrapolation.

CONCLUSIONS

This study has explored the feasibility of using friction pendulum bearings for seismic isolation of rigid storage tanks. The dynamic analysis of rigid tanks implemented with sliding-type isolation systems is a highly non-linear problem due to the presence of frictions. An analytical model for seismically isolated cylindrical storage tanks has been derived and a solution algorithm developed, to assess the structural-hydrodynamic characteristics of such hybrid systems. The friction force is determined, with the extra conditions of equilibrium and kinematic compatibility at the sliding interfaces, by simple matrix algebraic analysis under the framework of state-space formulation. The structural-hydrodynamic responses are thus obtained recursively with a one-step correction strategy, and a constant integration step size can be used throughout the analysis, without slowing down even near the stick–slip transitions. Numerical simulations

have been performed using the 1940 El Centro Earthquake as the input. Based on the simulation results, it can be concluded that

(1) The hydrodynamic pressure of the tank–liquid system during earthquakes is mainly caused by the impulsive component rather than the convective component, and the proportion of the impulsive pressure in the overall hydrodynamic pressure increases with H/R.
(2) Seismic isolation can effectively reduce the impulsive dynamic pressure while barely affecting the convective dynamic pressure.
(3) The efficiency of seismic isolation control, in terms of peak reduction in base shear or overturning moment, increases with PGA/μg. For a specified frictional coefficient of the sliding bearings, isolation effect increases with earthquake strength; or conversely, for a specified earthquake intensity, isolation effect increases as frictional coefficient declines. Peak reduction of up to 80 per cent can be achieved.
(4) The efficiency of seismic isolation control increases with H/R. For a specified PGA/μg, the larger the H/R ratio implies a better isolation effect, while larger displacement of the bearings is demanded as a trade-off.

ACKNOWLEDGEMENTS

The authors would like to thank the National Science Council of the Republic of China for financially supporting this research under Grant No. NSC 89-2211-E-009-011.

REFERENCES

1. Liu WK, Uras RA. Transient failure analysis of liquid-filled shells, part I: theory. *Nuclear Engineering and Design* 1989; **117**:107–139.
2. Liu WK, Uras RA. Transient failure analysis of liquid-filled shells, part II: applications. *Nuclear Engineering and Design* 1989; **117**:141–157.
3. Uras RA, Liu YK. Dynamic buckling of liquid-filled shells under horizontal excitation. *Journal of Sound and Vibration* 1990; **141**(3):389–408.
4. Zayas VA, Low SS. Application of seismic isolation to industrial tanks. PVP-*Seismic*, *Shock*, *and Vibration Isolation ASME* 1995; **319**:273–288.
5. Haroun MA, Housner GW. Seismic design of liquid storage tanks. *Journal of Technical Councils ASCE* 1981; **107**, TC1:191–207.
6. Haroun MA, Housner GW. Dynamic characteristics of liquid storage tanks. *Journal of Engineering and Mechanical Division ASCE* 1982; **108**, EM5:783–818.
7. Veletsos AS. Seismic response and design of liquid storage tanks. Guidelines for the seismic design of oil and gas pipeline systems. *Technical Council on Lifeline Earthquake Engineering ASCE* NY 1984:255–370, 443–461.
8. Veletsos AS, Tang Y, Tang HT. Dynamic response of flexibly supported liquid-storage tanks. *Journal of Structural Engineering ASCE* 1992; **118**(1):264–283.
9. Veletsos AS, Shivakumar P. Sloshing response of layered liquids in rigid tanks. *Earthquake Engineering and Structural Dynamics* 1993; **22**(9):801–821.
10. Veletsos AS, Shivakumar P. Hydrodynamic effects in rigid tanks containing layered liquids. *Earthquake Engineering and Structural Dynamics* 1995; **24**(6):835–860.
11. Craig RR. *Structural dynamics—an introduction to computer methods.* Wiley: New York, 1981.
12. Wang YP, Chung, LL, Liao WH. Seismic response analysis of bridges isolated with friction pendulum bearing. *Earthquake Engineering and Structural Dynamics* 1998; **27**:1069–1093.
13. Wang YP, Liao WH. Dynamic analysis of sliding structures with unsynchronized support motions. *Earthquake Engineering and Structural Dynamics* 2000; **29**:297–313.

